How is the balance of a forecast ensemble affected by adaptive and non-adaptive localization schemes?

20th October 2014

Ross Bannister, Stefano Migliorini, Laura Baker and Ali Rudd

Abstract

This paper investigates the effect on balance of a number of Schur product-type localization schemes which have been designed with the primarily function of reducing spurious far-field correlations in forecast error statistics. The localization schemes studied are a mixture of a non-adaptive scheme (where the moderation matrix is decomposed in a spectral basis), and two adaptive schemes, namely a simplified version of SENCORP (Smoothed ENsemble COrrelations Raised to a Power) and ECO-RAP (Ensemble COrrelations Raised to A Power). The paper shows, we believe for the first time, how the degree of balance (geostrophic and hydrostatic) implied by the error covariance matrices localized by these schemes can be diagnosed. Here it is considered that an effective localization scheme is one that reduces spurious correlations adequately but also minimizes disruption on balance (where the 'correct' degree of balance is assumed to be possessed by the unlocalized ensemble). By varying free parameters that describe each scheme (e.g. the degree of truncation in the schemes that use the spectral basis, the 'order' of each scheme, and the degree of ensemble smoothing), it is found that a particular configuration of the ECO-RAP scheme is best suited to the convective-scale system studied. According to our diagnostics, geostrophic balance is closely maintained by this scheme, but hydrostatic balance is weakened at many vertical levels, although less so than other configurations and than the other schemes.

1 Introduction

1.1 Sampling error

Progress to improve the efficacy of ensemble data assimilation (DA) methods like the ensemble Kalman filter (EnKF) has been impeded by problems with sampling error, which arises from finite ensemble sizes (N members), especially those ensembles that are small compared to the size of the system (n elements in the state vector), see e.g. [11, 10, 12]. Sampling error appears in calculations of an ensemble-derived estimate of the forecast error covariance matrix $\mathbf{P}^{\mathrm{DE}}_{(N)} \in \mathbb{R}^{n\times n}$. The standard form of this matrix is:

$$\mathbf{P}^{\mathrm{DE}}_{(N)} = \frac{1}{N-1}\sum_{l=1}^{N} \delta\mathbf{x}_l \delta\mathbf{x}_l^{\mathrm{T}} = \frac{1}{N-1}\mathbf{X}\mathbf{X}^{\mathrm{T}}, \tag{1}$$

where the superscript "DE" stands for "dynamical ensemble" (produced directly from the dynamical model - see Tab. 1), $\delta\mathbf{x}_l \in \mathbb{R}^n$ is the lth perturbation from the ensemble mean, and

Ensemble	Description	No. of members	Ensemble member	Ensemble matrix	Covariance
Dynamical ensemble (DE)	The ensemble of perturbations from the dynamical forecast model (pre-localization).	N	$\delta\mathbf{x}_l$	$\mathbf{X}$	$\mathbf{P}^{\mathrm{DE}}_{(N)}$
Correlation function ensemble (CE)	The ensemble whose covariance gives the correlation matrix that localizes.	K	$\boldsymbol{\omega}_k$	$\mathbf{K}$	$\boldsymbol{\Omega}^{\mathrm{CE}}_{(K)}$
Localized ensemble (LE)	The ensemble whose covariance gives the localized covariances.	M	$\tilde{\mathbf{x}}_m$	$\tilde{\mathbf{X}}$	$\mathbf{P}^{\mathrm{LE}}_{(N,K)}$
Smoothed ensemble (SE)	A spatially smoothed version of the dynamical ensemble.	N	$\delta\mathbf{w}_l$	—	$\mathbf{C}$

Table 1: Summary of the four types of ensemble used in this paper. The "correlation function" and "localized" ensembles are specified with either the spectral, SENCORP or ECO-RAP schemes.

$\mathbf{X} \in \mathbb{R}^{n\times N}$ is the matrix of ensemble perturbations $\mathbf{X} = \{\delta\mathbf{x}_1, \delta\mathbf{x}_2, \ldots \delta\mathbf{x}_N\}$. We shall call the ensemble comprising the N members $\delta\mathbf{x}_l$ the DE. Due to sampling error, this is only an estimate of the true forecast error covariance matrix $\mathbf{P}$. The following formula provides a rough guide to how sampling error in the correlation $\left[\mathbf{C}^{\mathrm{DE}}_{(N)}\right]_{ij} = \left[\mathbf{P}^{\mathrm{DE}}_{(N)}\right]_{ij} / (\sigma_i\sigma_j)$ (denoted $\left[\mathcal{E}\left\{\delta\mathbf{C}^{\mathrm{DE}}_{(N)}\right\}\right]_{ij}$) changes with N and the true correlation $\mathbf{C}$:

$$\left[\mathcal{E}\left\{\delta\mathbf{C}^{\mathrm{DE}}_{(N)}\right\}\right]_{ij} \sim \frac{1}{\sqrt{N}}\left(1 - \left([\mathbf{C}]_{ij}\right)^2\right), \tag{2}$$

[11] where i and j are component indices, $[\bullet]_{ij}$ indicates a matrix element and σ_i is the standard deviation of component i, $\sigma_i^2 = [\mathbf{P}]_{ii}$. Apart from the well-known dependence of sampling error on N, the other feature of this expression is that sampling errors are expected to be high when true correlations $\mathbf{C}_{ij}$ are small. Such sampling errors in the EnKF lead to anomalous analysis increments especially in the far-field - e.g. between an observation and distant fields where expected true correlations are small - and to anomalous covariances in observation space through the term $\mathbf{HPH}^{\mathrm{T}}$ in the analysis equations. The beauty of the EnKF over traditional variational schemes is that no covariance model is needed and so does not fall foul of incorrect assumptions that may be made in that covariance model (namely assumptions of homogeneity, isotropy, and geostrophic and hydrostatic balances) which may not be valid. This is though at the cost of sampling error.

1.2 Localization

In general it is not possible to distinguish genuinely large values of sample covariances from anomalously large ones that arise due to sampling error, but it is often possible to reduce sampling errors by damping covariances that are expected to be small. For instance, if points i and j are separated by a large distance then they may be expected to be only weakly correlated. By this reckoning these sample covariances should be damped or eliminated. This is the idea behind localization, where the elements $[\mathbf{P}^{\mathrm{DE}}_{(N)}]_{ij}$ are effectively multiplied by a moderation function, λ, which is unity when $i = j$ and reduces with increased separation between the locations represented by i and j ($\mathbf{r}_i$ and $\mathbf{r}_j$ respectively).

There are a number of ways that localization may be applied in ensemble DA. The Schur (element-by-element) product method replaces $\mathbf{P}^{\mathrm{DE}}_{(N)}$ in the EnKF with a localized version, $\mathbf{P}^{\mathrm{LE}}_{(N,K)} = \mathbf{P}^{\mathrm{DE}}_{(N)} \circ \mathbf{\Omega}^{\mathrm{CE}}_{(K)}$, where $\mathbf{\Omega}^{\mathrm{CE}}_{(K)} \in \mathbb{R}^{n\times n}$ is the moderation matrix formed of moderation functions (for a single field, $[\mathbf{\Omega}^{\mathrm{CE}}_{(K)}]_{ij} = \mu(\mathbf{r}_i, \mathbf{r}_j)$, where $|\mu(\mathbf{r}_i, \mathbf{r}_j)| \leq 1$ and $\mu(\mathbf{r}_i, \mathbf{r}_i) = 1$), [9]. The meanings of the "CE" superscript and the (K) subscript are explained in Sect. 2.1. The main issues with this method are in the choice of moderation function, in how it is implemented, and in any undesirable side effects of the localization, such as damage to filter's balance properties.

Localization can also be applied by limiting observations that contribute to each grid point to those that fall within a localization radius (domain localization). This is used, e.g., in the Local Ensemble Kalman Filter (LEKF) [5] and is commonly used with the Ensemble Transform Kalman Filter (ETKF) [13] and the Singular Evolutive Interpolated Kalman filter (SEIK filter) [14]. Domain localization can give rise to loss of smoothness [15] and is problematic for observations whose observation operators are a function of a highly non-local part of the model space (such as measurements from radiometers) [16, 2, 4]. The focus of this paper is on the Schur product formulation and how it affects geophysical balances.

1.3 The effect of localization on geophysical balances

Localization helps to alleviate some of the sampling noise problems with ensemble DA, but they can degrade essential geophysical balance properties of the ensemble. This was demonstrated by [19] who showed that anomalous rapid oscillations in surface pressure appeared in the (localized) EnKF analyses.

Inappropriate imbalance is known to be very damaging to subsequent forecasts and so methods have been sought to reduce this effect. The simplest approach is to weaken the effect of the localization by choosing moderation functions with longer length-scales [19], but this lessens the benefit of localization, and so requires more ensemble members. In any case, other factors - such as the information provided by observations - influence the localization length-scales that should be used [20]. It has been suggested that the root cause of balance degradation is due to distortion of the covariance structures by the moderation functions [12, 22]. This affects mostly those variables that are strongly anisotropic [22] like u and v (the zonal and meridional winds - see e.g. Fig. 3 of [21]). In [22], the analysis is performed in terms of the more isotropic ψ and χ (streamfunction and velocity potential) instead of u and v, which was found to maintain a well balanced ensemble. The Met Office's hybrid DA scheme [24] localizes the same variables that are used in their variational data assimilation system [23], namely increments of ψ, χ, p_{u} (unbalanced pressure) and μ (relative humidity). Balance is then introduced explicitly by the parameter transform in their control variable transform[1], which gives increments of u, v, p (total pressure), θ (potential temperature) and q (specific humidity). The parameter transform enforces balance conditions explicitly.

Although these are successful methods to maintain balance, they are likely to have limitations in their applicability in DA. The approach of [24] requires that the appropriate balances (in this case strong hydrostatic balance and weak geostrophic balance) are appropriate for the system. These are questionable for convective flows where, contrary to the large-scale case, adding balance may be damaging. The approach of [22] does not add geostrophic balance artificially, but it is unclear how it can be applied to preserve hydrostatic balance where the (unknown) equivalent of an 'isotropic' variable in the vertical is needed. For these reasons we turn to some adaptive localization schemes applied to the original variables (u, v, etc.), and use them with a convective-scale ensemble to see how they affect balance.

[1] The parameter transform is called the balance operator in some DA systems.

1.4 Static vs. adaptive localization schemes

Traditionally moderation functions are prescribed and do not change with the flow, but over recent years schemes have been proposed that generate moderation functions which change with the flow. Here we examine some properties of a number of static and adaptive localization schemes on a test ensemble. The adaptive schemes studied are a simplified version of SENCORP (Smoothed ENsemble COrrelations Raised to a Power) [3] and two variants of ECO-RAP (Ensemble COrrelations Raised to A Power) [1]. The properties that we will examine for each scheme are (i) the structure of the moderation functions and (ii) the effect on the degree of balance.

1.5 The cases studied

The main test ensemble is a 24-member ensemble of 3-hour forecasts from a quasi-operational high-resolution weather forecasting model (the Met Office's 1.5 km now-casting model with a domain over the Southern UK [30]). The ensemble's analysis perturbations are produced by MOGREPS (the Met Office Global and Regional Ensemble Prediction System [17] adapted for this domain [25, 26]). The date chosen as the main test is 20th September 2011, when a cold front passed over the Southern UK. This case is interesting as the flow shows detectable deviations from geostrophic and hydrostatic balances and so should provide a good test of a localization scheme to preserve the balance of the DE. Details of this case are documented in [18]. A second case is studied to test further some of the results, which is a 24-member ensemble of 1-hour forecasts. The date chosen for the second test is 26th July 2007, which has regions of convective precipitation. Details of this second case are documented in [25, 28]. It is beyond the scope of this paper to run DA with these cases, but the balance diagnostics shown should be useful to guide the choice of localization scheme for DA.

The structure of this paper is as follows. In Sect. 2 we review the Schur product to define our notation and describe each of the three localization schemes considered. In Sect. 3 we introduce and derive a range of diagnostics that show how each scheme localizes and affects balance for the main case study. In Sect. 4 we use the best of the schemes found and apply them to other profiles (including for the second case study). In Sect. 5 we discuss the results and limitations of the present work, conclude the paper and suggest further work.

2 The localization schemes

In this section the Schur product localization is described, and two static and three adaptive variants of localization schemes are described.

2.1 Schur-product localized covariances

Just as $\mathbf{P}^{\mathrm{DE}}_{(N)}$ can be written as the outer product of a set of ensemble members in (1), the matrix, $\boldsymbol{\Omega}^{\mathrm{CE}}_{(K)}$, as used in $\mathbf{P}^{\mathrm{LE}}_{(N,K)} = \mathbf{P}^{\mathrm{DE}}_{(N)} \circ \boldsymbol{\Omega}^{\mathrm{CE}}_{(K)}$ can be written in a similar way:

$$\boldsymbol{\Omega}^{\mathrm{CE}}_{(K)} = \frac{1}{K-1} \sum_{k=1}^{K} \boldsymbol{\omega}_k \boldsymbol{\omega}_k^{\mathrm{T}} = \frac{1}{K-1} \mathbf{K}\mathbf{K}^{\mathrm{T}}, \tag{3}$$

where $\boldsymbol{\omega}_k \in \mathbb{R}^n$ form a set of K new ensemble members that we shall call the "correlation function ensemble" (CE) (as $\boldsymbol{\Omega}^{\mathrm{CE}}_{(K)}$ behaves as a correlation matrix)[2]. The matrix $\mathbf{K} \in \mathbb{R}^{n \times K}$ is the matrix of the K CE members $\mathbf{K} = \{\boldsymbol{\omega}_1, \boldsymbol{\omega}_2, \dots \boldsymbol{\omega}_K\}$, and this matrix may be considered to be a 'square-root' of $\boldsymbol{\Omega}^{\mathrm{CE}}_{(K)}$. Each localization scheme that we consider will be decomposed into

[2] The terms "dynamical ensemble" and "correlation function ensemble" are adopted from [4].

its CE, which will help diagnose some of its important properties. From (1) and (3) the i, jth matrix elements of $\mathbf{P}^{\mathrm{DE}}_{(N)}$ and $\mathbf{\Omega}^{\mathrm{CE}}_{(K)}$ are, respectively:

$$[\mathbf{P}^{\mathrm{DE}}_{(N)}]_{ij} = \frac{1}{N-1}\sum_{l=1}^{N}[\delta\mathbf{x}_l]_i[\delta\mathbf{x}_l]_j, \text{ and } [\mathbf{\Omega}^{\mathrm{CE}}_{(K)}]_{ij} = \frac{1}{K-1}\sum_{k=1}^{K}[\boldsymbol{\omega}_k]_i[\boldsymbol{\omega}_k]_j, \tag{4}$$

where $[\bullet]_i$ indicates vector element. The CF ensemble must have the property that $[\mathbf{\Omega}^{\mathrm{CE}}_{(K)}]_{ii} = 1$, i.e. that the sum of squares (over the K members) of each element of the CE must equal to $K-1$. From (4) the i, jth element of $\mathbf{P}^{\mathrm{LE}}_{(N,K)}$ is:

$$\begin{aligned}
[\mathbf{P}^{\mathrm{LE}}_{(N,K)}]_{ij} &= [\mathbf{P}^{\mathrm{DE}}_{(N)}]_{ij}[\mathbf{\Omega}^{\mathrm{CE}}_{(K)}]_{ij}, \\
&= \frac{1}{(N-1)(K-1)}\sum_{l=1}^{N}\sum_{k=1}^{K}[\delta\mathbf{x}_l]_i[\boldsymbol{\omega}_k]_i\,[\delta\mathbf{x}_l]_j[\boldsymbol{\omega}_k]_j, \\
&= \frac{1}{(M-1)}\sum_{m=1}^{M}\tilde{\mathbf{x}}_m\tilde{\mathbf{x}}_m^{\mathrm{T}},
\end{aligned} \tag{5}$$

where $\tilde{\mathbf{x}}_m = \sqrt{\frac{M-1}{(N-1)(K-1)}}\delta\mathbf{x}_l \circ \boldsymbol{\omega}_k \in \mathbb{R}^n$ form a new set of M ensemble members that we shall call the "localized ensemble" (LE) where $M = NK$ and m is shorthand for every pair of l and k that appears in the line above (5). The matrix whose columns are the LE members may be denoted $\tilde{\mathbf{X}} \in \mathbb{R}^{n\times M}$. The LE comprises every possible 'Schur product' pair of DE and CE members. Table 1 summarises this terminology. The increase in the number of members from N in the DE to M in the LE will lead to $\mathrm{rank}(\mathbf{P}^{\mathrm{LE}}_{(N,K)}) > \mathrm{rank}(\mathbf{P}^{\mathrm{DE}}_{(N)})$, and thus have a lower sampling error. The importance of (5) is that any diagnostic that is applied to the DE may be applied also to the LE, including the balance diagnostics to be introduced in Sect. 3.

2.2 Spectral representation of a localization matrix

Before the schemes are introduced it is useful to define how the static moderation functions are defined for a single variable s (where s in this paper represents either errors in zonal wind (δu), meridional wind (δv), pressure (δp) or temperature (δT)). Note that the scheme described here is denoted "spectral" because the localization matrix is represented in a spectral basis; it does not mean that localization has been done in spectral space.

2.2.1 Form of the square-root of the localization matrix

The correlation function matrix for the case of variable s, $\mathbf{\Omega}^{\mathrm{CE},s}_{(K)}$ needs to be represented as a 'square-root', $\mathbf{K}_s$. For the static schemes considered in this paper, the eigen-representation, $\mathbf{\Omega}^{\mathrm{CE},s}_{(K)} = \frac{1}{K-1}\mathbf{F}_s\mathbf{\Lambda}_s\mathbf{F}_s^{\mathrm{T}}$ is useful. The diagonal matrix $\mathbf{\Lambda}_s \in \mathbb{R}^{K\times K}$ comprises K non-zero eigenvalues, and $\mathbf{F}_s \in \mathbb{R}^{n\times K}$ comprises the eigenvectors. This is a rank K matrix (in practice $K \ll n$) which corresponds to $\mathbf{K}_s = \mathbf{F}_s\mathbf{\Lambda}_s^{1/2}$, which is this variable's CE (it also needs to be normalized so that the sum of squares of each row is $K-1$).

2.2.2 The horizontal and vertical bases used in this work

Columns of $\mathbf{F}_s$ comprise 3-D fields which are the products of horizontal plane waves and vertical modes (see below), and diagonal elements of $\mathbf{\Lambda}_s$ comprise a variance spectrum. The variance spectrum is a prescribed function of the horizontal total wavenumber of the plane waves and of

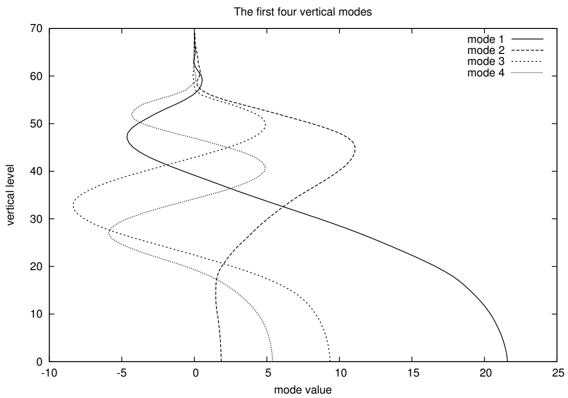

Figure 1: The first four vertical modes used as basis functions to represent vertical aspects of the moderation matrix in many of the localization schemes.

the vertical mode index. The elements of $\mathbf{K}_s$ are then:

$$[\mathbf{K}_s]_{\mathbf{rk}} = \underbrace{\cos\left(\frac{\pi}{L_x}k_x r_x + \delta_s^x\right)\cos\left(\frac{\pi}{L_y}k_y r_y + \delta_s^y\right)\nu\left(r_z, k_z\right)}_{[\mathbf{F}_s]_{\mathbf{rk}}}\underbrace{\lambda_s^{\mathrm{H}}\left(k_x^2 + k_y^2\right)\lambda_s^{\mathrm{V}}\left(k_z\right)}_{\left[\mathbf{\Lambda}_s^{1/2}\right]_{\mathbf{kk}}}, \qquad (6)$$

where the horizontal domain has dimensions $L_x \times L_y$. The subscripts on $[\mathbf{K}_s]_{\mathbf{rk}}$ have the following meanings: $\mathbf{r}$ represents a 3-D position r_x, r_y, r_z and $\mathbf{k}$ represents horizontal wavenumbers k_x, k_y and vertical mode k_z ($k_x, k_y, k_z \in \mathbb{Z}$). $\nu(r_z, k_z)$ is the value of k_zth vertical mode at level r_z. $\lambda_s^{\mathrm{H}}(k_x^2 + k_y^2)$ is the square-root of the horizontal part of the variance spectrum (a function of total horizontal wavenumber), and $\lambda_s^{\mathrm{V}}(k_z)$ is the square-root of the vertical part of the variance spectrum. The variance spectrum is prescribed to yield the required horizontal and vertical localization length-scales.

The phases δ_s^x and δ_s^y are chosen with the intention of allowing s to satisfy the imposed boundary conditions consistent with the limited area model. For wind components $\delta_{\delta u}^x = -\pi/2$, $\delta_{\delta u}^y = 0$, $\delta_{\delta v}^x = 0$ and $\delta_{\delta v}^y = -\pi/2$, which do not permit flow in or out of the domain. The remaining variables have $\delta_s^x = -\pi/2$ and $\delta_s^y = -\pi/2$, which represent zero Dirichlet boundary conditions. These conditions, however, are not seen in the correlations implied by (6) due to the normalization mentioned in Sect. 2.1 (see Sect. 3.2). Form (6) is valid for a continuous system and adjustments to (6) are needed to respect the staggering on the Arakawa C grid used for the Met Office model (not shown).

The vertical modes are mutually orthogonal[3] eigenvectors of a vertical error covariance matrix for the Met Office's unbalanced pressure control variable[4] used in the Met Office convective-scale variational DA system[23, 6]. The first four vertical modes are plotted in Fig. 1.

For the static localization scheme defined by $\mathbf{K}_s$ the adoption of plane waves in (6) and a variance spectrum dependent on the total horizontal wavenumber implies moderation functions for s in the horizontal that are homogeneous and isotropic (see e.g. Appendix A of [27]).

[3]The modes are orthogonal in a specific inner product $g(r_z)$, i.e. $\sum_{r_z=1}^{n_z}\nu(r_z, k_z)\nu(r_z, k_z')g(r_z) = \delta_{k_z k_z'}$.

[4]Modes for the 'unbalanced pressure' control variable are chosen as a convenient basis as they have reasonable properties for this work, namely that the amplitude of their oscillations tend to decay with altitude.

2.2.3 The horizontal and vertical variance spectra

To derive the horizontal and vertical variance spectra, we first define the following:

$$\mu^{\mathrm{H}}(\mathbf{r}_{\mathrm{H}_1}, \mathbf{r}_{\mathrm{H}_2}) = \exp - \left(\frac{|\mathbf{r}_{\mathrm{H}_2} - \mathbf{r}_{\mathrm{H}_1}|}{\hat{\ell}_{\mathrm{H}}} \right)^2, \tag{7}$$

$$\mu^{\mathrm{V}}(r_{z_1}, r_{z_2}) = \exp - \left(\frac{r_{z_2} - r_{z_1}}{\hat{\ell}_{\mathrm{V}}} \right)^2, \tag{8}$$

where $\hat{\ell}_{\mathrm{H}}$ and $\hat{\ell}_{\mathrm{V}}$ are the horizontal and vertical length-scales respectively and $\mathbf{r}_{\mathrm{H}} = \begin{pmatrix} r_x & y_y \end{pmatrix}$. Equations (7) and (8) are the horizontal and vertical moderation functions approximated by the spectral localization scheme (they are also used in the ECO-RAP scheme, but not in SENCORP). The combined localization is $\mu = \mu^{\mathrm{H}}\mu^{\mathrm{V}}$ and they are functions that decay with horizontal and vertical separation.

The λ_s^{H} spectrum is found by projecting (7) onto the plane waves (i.e. a Fourier transform), and the λ_s^{V} spectrum is found by projecting (8) onto the vertical modes. Given that $K \ll n$, (K is the product of the number of plane waves and the number of vertical modes) these spectra will be highly truncated, and so a localization scheme that is based on (6) will not perfectly recover forms (7) and (8). For this reason in each experiment in Sect. 3 we describe the length-scales as those that are implied from the spectral scheme - denoted ℓ_H and ℓ_{V} (without hats) - rather than the prescribed length-scales in (7) and (8).

2.3 The static (spectral) localization scheme

Equation (6) forms the basis of a univariate static localization scheme where the moderation functions are parametrized as defined in (7) and (8). The extension to multivariate static localization schemes is necessary to study balance. The scheme is summarised with the following form of the moderation ensemble:

$$\mathbf{K}^{\mathrm{Spec}} = \overline{\begin{pmatrix} \mathbf{F}_{\delta u}\boldsymbol{\Lambda}_{\delta u}^{1/2} \\ \mathbf{F}_{\delta v}\boldsymbol{\Lambda}_{\delta v}^{1/2} \\ \mathbf{F}_{\delta p}\boldsymbol{\Lambda}_{\delta p}^{1/2} \\ \mathbf{F}_{\delta T}\boldsymbol{\Lambda}_{\delta T}^{1/2} \end{pmatrix}} \in \mathbb{R}^{n\times K}, \tag{9}$$

$$[\mathbf{K}^{\mathrm{Spec}}]_{(\mathbf{r}s)\mathbf{k}} = [\boldsymbol{\omega}_{\mathbf{k}}]_{(\mathbf{r}s)} = c_{(\mathbf{r}s)}[\mathbf{F}_s]_{\mathbf{r}\mathbf{k}}[\boldsymbol{\Lambda}_s^{1/2}]_{\mathbf{k}\mathbf{k}}. \tag{10}$$

where K is the number of modes used for each variable. The over-bar in (9) indicates that the matrix is normalized such that the sum of squares of each row must be $K-1$ (see Sect. 2.1), which is accounted for by the normalizing factor $c_{(\mathbf{r}s)}$ in (10). The CE localization matrix, $\boldsymbol{\Omega}_{(K)}^{\mathrm{CE}}$, implied by (9) has auto-localization sub-matrices for variable s of the form $\mathbf{F}_s\boldsymbol{\Lambda}_s\mathbf{F}_s^{\mathrm{T}}$ (ignoring normalization), and cross-localization sub-matrices between variables s_1 and s_2 of the form $\mathbf{F}_{s_1}\boldsymbol{\Lambda}_{s_1}^{1/2}\boldsymbol{\Lambda}_{s_2}^{1/2}\mathbf{F}_{s_2}^{\mathrm{T}}$.

2.4 The adaptive localization schemes

The non-adaptive localization scheme is based on the spectral method described in Sects. 2.2 and 2.3 which does not change with the flow. The SENCORP and ECO-RAP-based schemes on the other hand are flow dependent. SENCORP is itself based purely on the ensemble and ECO-RAP is based on a combination of the ensemble and the spectral method.

2.4.1 The simplified SENCORP localization scheme

In the simplified version of the 'order-Q' SENCORP scheme [3] that is studied in this paper, the moderation matrix is taken to have the form[5]:

$$\mathbf{\Omega} = \mathbf{C}^{\circ Q}, \tag{11}$$

where $\circ Q$ means the 'Schur power' (the Schur product of Q $\mathbf{C}$-matrices, $Q > 0$). The matrix $\mathbf{C} \in \mathbb{R}^{n \times n}$ is the correlation matrix formed from N spatially smoothed versions of the original ensemble members, $\delta \mathbf{w}_l$ ($1 \leq l \leq N$), and are collectively called the "smoothed ensemble" (SE) - Tab. 1. The members are normalized after smoothing such that the variance of each element amongst the SE is $N-1$ to ensure that the diagonal elements of $\mathbf{C}$ - and hence $\mathbf{C}^{\circ Q}$ - are unity. $\mathbf{C}$ is then found from $\mathbf{C} = \frac{1}{N-1} \sum_{l=1}^{N} \delta \mathbf{w}_l \delta \mathbf{w}_l^{\mathrm{T}}$. A square-root of $\mathbf{\Omega}$ may be formed as a generalisation of (5). The i,jth element of $\mathbf{\Omega}$ is:

$$\begin{aligned}
\mathbf{\Omega}_{ij} = (\mathbf{C}_{ij})^{Q} &= \left(\frac{1}{N-1} \right)^{Q} \left(\sum_{l=1}^{N} [\delta \mathbf{w}_l]_i [\delta \mathbf{w}_l]_j \right)^{Q}, \\
&= \left(\frac{1}{N-1} \right)^{Q} \sum_{l_1=1}^{N} \cdots \sum_{l_Q=1}^{N} [\delta \mathbf{w}_{l_1}]_i \ldots [\delta \mathbf{w}_{l_Q}]_i \, [\delta \mathbf{w}_{l_1}]_j \ldots [\delta \mathbf{w}_{l_Q}]_j, \\
&= \frac{1}{(K-1)} \sum_{k=1}^{K} [\boldsymbol{\omega}_k]_i [\boldsymbol{\omega}_k]_j,
\end{aligned} \tag{12}$$

where the kth SENCORP CE member is $\boldsymbol{\omega}_k = \sqrt{\frac{K-1}{(N-1)^Q}} \delta \mathbf{w}_{l_1} \circ \ldots \circ \delta \mathbf{w}_{l_Q}$ and where $K = N^Q$ is the number of SENCORP moderation members and k is shorthand for every combination of $l_1 \ldots l_Q$ that appears in the line above (12). The matrix containing the CE members is denoted $\mathbf{K}^{\mathrm{SENCORP}} \in \mathbb{R}^{n \times N^Q}$. The smoothing step is performed to give correlation length scales in $\mathbf{C}$ that are longer than those in $\mathbf{P}_{(N)}^{\mathrm{DE}}$. The degree of smoothing is chosen, and the price of overestimating the smoothing length-scales is only to lead to a less efficient method[6]. The Schur power of Q acts to reduce correlations most amongst the SE that are small (these correlations arguably should be zero, but may not be zero because of sampling noise), but maintains correlations that are close to ± 1. In order to preserve the sign of the sample covariances during the localization, Q must be even[7]. The definition of SENCORP's CE in terms of the ensemble is the key adaptive feature of this method. Once the CE is found, the LE follows from (5).

2.4.2 The ECO-RAP localization scheme

The matrix $\mathbf{K}^{\mathrm{ECORAP}}$ for the 'order-Q' ECO-RAP method [1] is a mixture of the SENCORP and spectral approaches:

$$\mathbf{K}^{\mathrm{ECORAP}} = \overline{\mathbf{C}^{\circ Q} \begin{pmatrix} \mathbf{F}_{\delta u} \mathbf{\Lambda}_{\delta u}^{1/2} \\ \mathbf{F}_{\delta v} \mathbf{\Lambda}_{\delta v}^{1/2} \\ \mathbf{F}_{\delta p} \mathbf{\Lambda}_{\delta p}^{1/2} \\ \mathbf{F}_{\delta T} \mathbf{\Lambda}_{\delta T}^{1/2} \end{pmatrix}} \in \mathbb{R}^{n \times K}, \tag{13}$$

[5] The full SENCORP localization matrix in [3] is $[(\mathbf{C}^{\circ Q})^q]^{\circ r}$, but this is too difficult to factorise for the large state space studied in this paper. Our simplified application is the case $q = 1$ and $r = 1$.

[6] In the limit of infinitely long length-scales in $\mathbf{C}$, SENCORP will revert to the unlocalized system.

[7] Normally Q is even as indicated, but we will also consider a case when $Q = 1$ (in which case all matrix elements of $\mathbf{C}^{\circ Q}$ are replaced with their absolute values).

where the correlation matrix $\mathbf{C}^{\circ Q}$ is defined in Sect. 2.4.1. The number of CE members (the number of columns in $\mathbf{K}^{\text{ECORAP}}$) is the same as in $\mathbf{K}^{\text{Spec}}$, which depends on the number of horizontal plane waves and vertical modes. The matrix elements of (13) are:

$$[\mathbf{K}^{\text{ECORAP}}]_{(\mathbf{r}s)\mathbf{k}} = [\boldsymbol{\omega}_{\mathbf{k}}]_{(\mathbf{r}s)} = c_{(\mathbf{r}s)} \sum_{\mathbf{r}'s'} (\mathbf{C}^{\circ Q})_{(\mathbf{r}s)(\mathbf{r}'s')} \mathbf{F}_{(\mathbf{r}'s')\mathbf{k}} (\boldsymbol{\Lambda}_{s'}^{1/2})_{\mathbf{kk}}. \tag{14}$$

3 Diagnosed correlation functions and balance properties

The experiments performed for this work are listed in Tab. 2. The free parameters that are explored include the degree of truncation (via N_{k_x} and N_{k_z}), the implied horizontal and vertical length-scales (ℓ_{H} and ℓ_{V}, controlled by $\hat{\ell}_{\text{H}}$ and $\hat{\ell}_{\text{V}}$ in (7) and (8)), the degree of ensemble pre-smoothing, the order (Q) and the influence parameters (to be described in Sect. 3.4). Not all parameters are relevant to all schemes. There are two kinds of diagnostics shown in this paper:

- Spatial correlation functions (univariate and multivariate) are computed between a selection of variables calculated from members of the DE (1) and the LE (5). These are found from either the covariances $\mathbf{P}_{(N)}^{\text{DE}}$ for the unlocalized system, or $\mathbf{P}_{(N,K)}^{\text{LE}}$ for a localized system (normalized by the standard deviations in the usual way). Some of the spatial moderation functions found from $\boldsymbol{\Omega}_{(K)}^{\text{CE}}$ (3) are also shown. These show how strong the degree of localization is and how the schemes deal with multivariate aspects.
- Balance diagnostics that measure the degree of geostrophic and hydrostatic balance are computed for the dynamical and localized ensembles. These diagnostics are found as follows (see [28] for details):
  - For geostrophic balance (GB) the linear balance equation is used: $D\delta'/Dt = \mathcal{M}' + \mathcal{W}' +$ other terms, where δ' is the perturbation of divergence, and $\mathcal{M}'$ and $\mathcal{W}'$ are perturbations of the 'mass' and 'wind' terms respectively (Eqs. (3)-(5) of [28]). Perturbations are computed with respect to the mean. For flow in perfect GB (and assuming that the other terms are negligible), $\mathcal{M}'$ and $\mathcal{W}'$ will be exactly anti-correlated.
  - For hydrostatic balance (HB) the vertical wind equation is used: $Dw'/Dt = \mathcal{P}' + \mathcal{T}' +$ other terms, where w' is the perturbation of vertical wind, and $\mathcal{P}'$ and $\mathcal{T}'$ are perturbations of the 'vertical pressure gradient' and 'temperature' terms respectively (Eqs. (6)-(8) of [28]). For flow in perfect HB (and assuming that the other terms are negligible), $\mathcal{P}'$ and $\mathcal{T}'$ will be exactly anti-correlated.

3.1 Diagnostics of the dynamical ensemble (no localization)

We have computed a large number of correlation functions for each case study, but we show only a small selection of these to demonstrate the important points. Figure 2 shows some sample correlation functions from the DE (Exp. 0 in Tab. 2).

The first row, panels (a)-(c), are δT-δT spatial correlations on three cross sections through the domain (the correlations are between positions in the field and the cross-hair). At the validity time of the ensemble there is a cold front passing over the UK from the west and orientated along the SW-NE direction [18]. This is reflected in the anisotropy of the correlation structure in panel (a), which is at level 30 (overlaid ellipse). The sign of the correlations stays mostly positive in the horizontal, but there are some far-field features that may be due to sampling error. The vertical correlations, panels (b) and (c) show mainly positive correlations up to level 55 and have a band of negative correlations above that. The local correlation structure shows patterns that slope with longitude and latitude (overlaid ellipses). Some vertical correlations, especially those involving δT and δp, may have legitimate far-field correlations (which arise due

Exp	Scheme	N	N_{k_x}	N_{k_z}	N_{k_H}	ℓ_H	ℓ_V	Smoothing		Q	$\mathbf{C}^{\circ Q}$ influence		K
								Horiz	Vert		ρ_H	ρ_V	
0	None	24	—	—	—	—	—	—	—	—	—	—	—
1	Spectral	24	9	5	58	200	30	—	—	—	—	—	290
2	Spectral	24	9	5	58	100	30	—	—	—	—	—	290
3	SENCORP	16	—	—	—	—	—	0	0	1	—	—	16
4	SENCORP	16	—	—	—	—	—	0	0	2	—	—	256
5	SENCORP	16	—	—	—	—	—	0	0	4	—	—	65536
6	SENCORP	16	—	—	—	—	—	10	10	2	—	—	256
7	SENCORP	16	—	—	—	—	—	50	50	2	—	—	256
8	ECO-RAP	24	9	5	58	200	30	2	2	2	0	2	290
9	ECO-RAP	24	9	5	58	200	30	2	2	2	0	16	290
10	ECO-RAP	24	9	5	58	200	30	2	2	2	0	24	290
11	ECO-RAP	24	9	5	58	200	30	2	2	2	0	32	290
12	ECO-RAP	24	9	5	58	200	30	2	2	2	0	64	290
13	ECO-RAP	24	9	5	58	200	30	2	2	1	0	24	290
14	ECO-RAP	24	9	5	58	200	30	2	2	4	0	24	290

Table 2: Summary of experiments used to study the effect of localization on balance. The variables N_{k_x} and N_{k_z} refer to the number of wavenumbers used in the x and z directions respectively (with $N_{k_y} = N_{k_x}$). The total number of horizontal wavenumbers, N_{k_H}, is found by counting the number of wavenumbers whose total horizontal wavenumber satisfies $\sqrt{k_x^2 + k_y^2} \leq N_{k_x}$. For comparison with K, the number of grid points representing one field is $\sim 360 \times 288 \times 70 \sim 7 \times 10^6$.

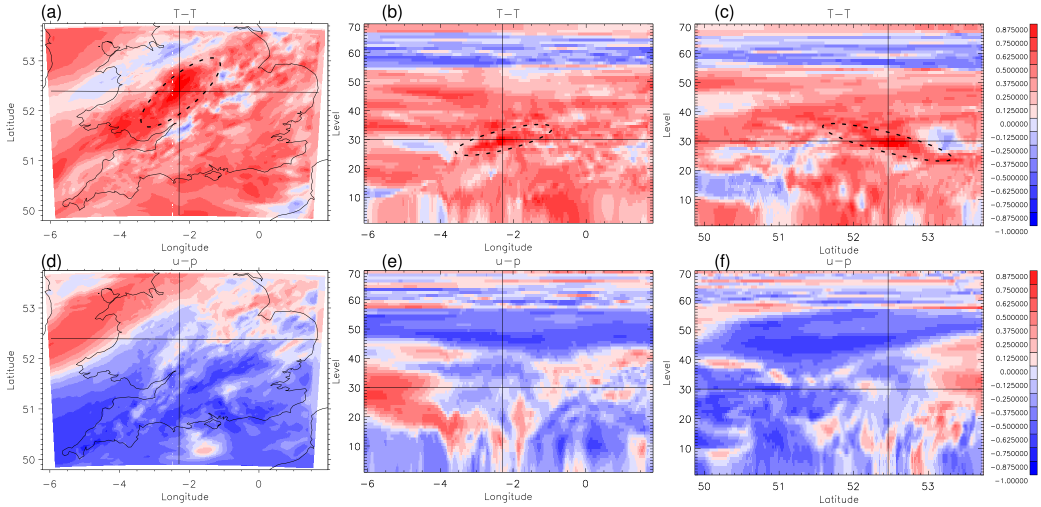

Figure 2: Univariate and multivariate spatial correlation functions for the main case study (20th September 2011, 15 UTC) with no localization (Exp. 0). The first row, (a)-(c), is for correlations of temperature at field locations with temperature at the cross-hair and the second row, (d)-(f) is for correlations of zonal wind at field locations with pressure at the cross-hair. The cross-sections correspond to the horizontal and vertical lines.

to 'action at a distance' effects caused by, e.g., near HB) so the effect of localization in the vertical requires special attention.

The second row, panels (d)-(e), are δu-δp spatial correlations (the correlations are between δu at positions in the field with δp at the cross-hair). On level 30, there are mainly positive correlations to the north and negative correlations to the south of the cross-hair, which is the large-scale pattern expected from GB [28, 21], although the pure geostrophic pattern is disturbed and the field is modulated strongly the front. The vertical cross-sections, panels (e) and (f), show large-scale and small-scale structures, but a clear band of negative correlation between levels ~ 45 and ~ 55. These features are examples of the structures that an ensemble brings to DA although the values in the far-field are likely to be noise.

The balance diagnostics corresponding to the vertical profile at the horizontal cross-hair position are shown in panels (a) and (b) of Fig. 3 (continuous lines). The geostrophic covariance diagnostic, panel (a), shows that GB is not well obeyed in the the DE, apart from around level 19. The low degree of GB is not surprising given that we are measuring GB at the grid scale and that a front is passing through. The hydrostatic diagnostic, panel (b), shows that HB is almost perfectly satisfied (values are only just distinguishable from the ordinate and note the different scales of the abscissa between the two panels), with slight deviations around levels 11, 20, 28, and 37. For the purposes of this paper, these balance diagnostics for the unlocalized system are considered as the target values which we would like preserved after localization.

Panels (c)-(e) of Fig. 3 (continuous lines) are the correlation functions for δT-δT in the longitude, latitude and vertical directions along the cross-hairs in panels (a)-(c) of Fig. 2. These will be useful for comparison with the localized correlation functions to assess the degree of localization of the schemes considered.

3.2 Diagnostics of the spectral scheme

The implied spatial moderation functions for δT-δT and δu-δp found from the CE for the spectral scheme using a modest number of wavenumbers ($N_{k_x} = 9$ and $N_{k_z} = 5$) are shown

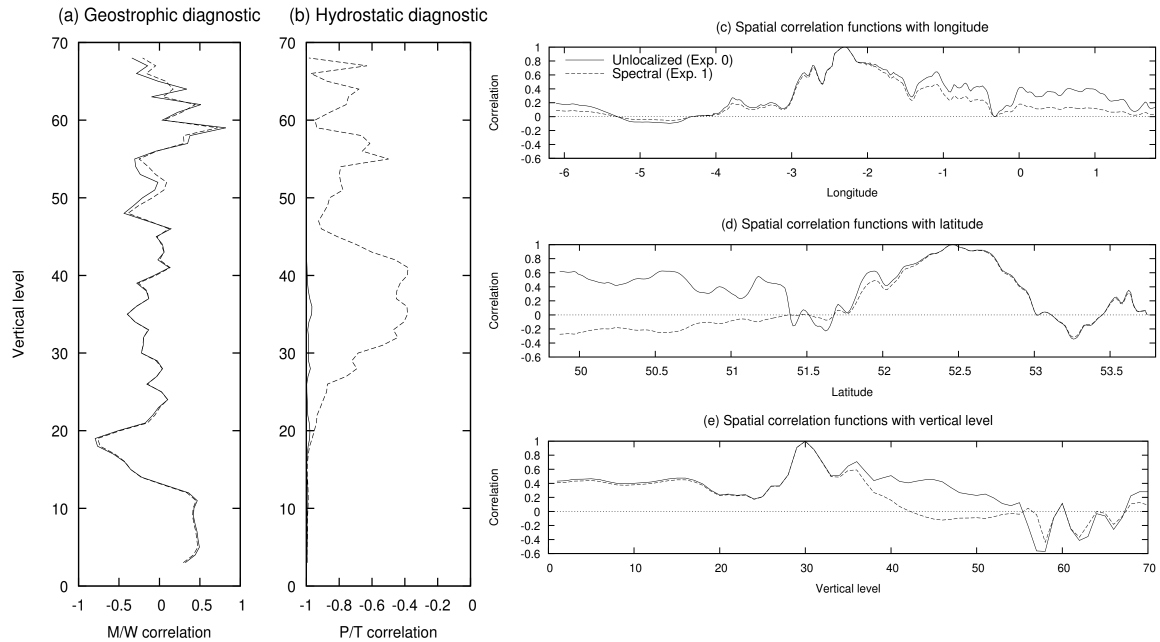

Figure 3: Diagnostics for the unlocalized and spectral scheme for the main case study. Panels (a) and (b): geostrophic and hydrostatic correlation diagnostics. Panels (c)-(e): spatial correlation functions with longitude, latitude and level. In all panels the continuous lines are for the unlocalized system (Exp. 0) and the dashed lines are for the spectral scheme (Exp. 1).

in Fig. 4 in panels (a)-(f). This is denoted Exp. 1 in Tab. 2. If the moderation functions were represented perfectly then the correlation functions for univariate correlations, panels (a)-(c), would be isotropic in the horizontal (in terms of grid-points rather than longitude and latitude) and monotonically decreasing away from the cross-hair to zero (in the vertical and in any horizontal direction), as (7) and (8). This is clearly not the case, as is highlighted by the presence of negative values. These are presumably features of the relatively low-rank CE (290 modes, which is much less than the number of grid points representing one field $\sim 7 \times 10^6$).

The implied moderation sub-matrix for δT-δT has the form $\mathbf{F}_{\delta T}\boldsymbol{\Lambda}_{\delta T}\mathbf{F}_{\delta T}^{\mathrm{T}}$ (Sect. 2.3), but for different variables, e.g. δu-δp, it has the form $\mathbf{F}_{\delta u}\boldsymbol{\Lambda}_{\delta u}^{1/2}\boldsymbol{\Lambda}_{\delta p}^{1/2}\mathbf{F}_{\delta p}^{\mathrm{T}}$. The vertical basis functions in $\mathbf{F}$, denoted $\nu(r_z, k_z)$ in (6), are the same for all variables in this work, but the horizontal basis functions depend upon each variable's lateral boundary conditions (Sect. 2.2.2). Panels (d)-(f) of Fig. 4 show the implied spatial moderation function between δu and δp, which show the subtle differences with panels (a)-(c)[8]. Clear from all the moderation functions is their separable nature between the horizontal and vertical directions.

The localized spatial correlations found from the LE of Exp. 1 are shown in panels (g)-(l). The correlations maintain the broad structures from the DE in Fig. 2, but are, by design, more compact. Comparing Figs. 4 and 2, one of the most striking effects of the negative moderation values is the narrowing of the vertical band of δT-δT correlations in the vertical, which may have a damaging effect on balance. The selection of localized multivariate correlations (panels (j)-(l)) keep their local structures, which is essential for the localized system to have any chance of maintaining balance.

For reference, panels (c)-(e) of Fig. 3 (dashed lines) are the localized correlation functions

[8]The implied moderation functions for δT-δT were intended to disappear on the boundaries. This is not evident in the Figs. because the normalization of the CE performed to make the localization matrix $\boldsymbol{\Omega}_{(K)}^{\mathrm{CE}}$ into a correlation matrix destroys this property.

for δT-δT in the longitude, latitude and vertical directions along the cross-hairs, which show more clearly how they differ from the unlocalized correlation functions (continuous lines). The two are similar in the horizontal, panels (c) and (d), within a degree or so from the cross-hair (where the correlation is unity), but the localization tends to be stronger (and negative) in the southerly direction than in the northerly direction, panel (d). The two lines are similar in the vertical, panel (e), within about 5 levels of the cross-hair, but there is virtually no localization from level 30 downwards.

The balance diagnostics for Exp. 1 are overlaid in panels (a) and (b) of Fig. 3 (dashed lines). For the GB diagnostic, the localized ensemble follows closely the unlocalized ensemble, which is an encouraging result, but not surprising given that ℓ_{H} is quite large. When the horizontal length-scale, ℓ_{H} is halved (Exp. 2, in Tab. (2)), the close agreement lessens as expected (not shown). The spectral scheme though dramatically loses the HB present in the unlocalized system. This is a surprising result given that the unlocalized and localized correlation functions are indistinguishable in the vicinity of the centre of the cross-hair - panel (e) - so the vertical derivatives used in the HB diagnostic might be expected to be similar. Using this scheme to localize in a convective-scale ensemble-based DA scheme may therefore anomalously induce convective storms where there are not any.

3.3 Diagnostics of the SENCORP scheme

The spectral scheme uses the same moderation functions, irrespective of the flow regime. SENCORP on the other hand constructs moderation functions that are determined purely from the DE. The simplified SENCORP scheme has a number of parameters that can be adjusted, namely the order, Q, and the degree of smoothing of the DE members to make the SE, which then make the CE as in (12). As for the spectral scheme in Sect. 3.2, we examine the appearance of the moderation functions and the effect that the scheme has on balance. For these SENCORP experiments, we limit the number of ensemble members to $N = 16$ (see below).

3.3.1 Effect of the order, Q

Figures 5 and 6 show the same selection of spatial moderation functions as in Sect. 3.2, but for SENCORP with $Q = 2$ and $Q = 4$ respectively (no pre-smoothing of the DE is performed at this stage and the unlocalized results shown use only 16 instead of 24 members). Panels (a)-(f) of these Figs. can be compared with the same panels in Fig. 4 for the spectral case (for brevity we do not show the SENCORP localized spatial correlations). For $Q = 2$ (Exp. 4) the degree of localization for temperature, panels (a)-(c) in Fig. 5 is more severe than for the spectral scheme studied. The structures in Fig. 5 are informed by the 'flow-of-the-day', but there is less freedom in the simplified SENCORP scheme to influence the length-scales. There are no anomalous negative correlations in the SENCORP results. The multivariate moderation functions that SENCORP applies between zonal wind and pressure, panels (d)-(e) of Fig. 5 are virtually zero at the same point (centre of the cross-hair), but can be significant elsewhere, especially south of the cross-hair. All regions of significant correlation are the same ones where the DE has significant correlation (Fig. 2). Increasing the order to $Q = 4$ (Exp. 5, Fig. 6) reproduces similar patterns as $Q = 2$, but with tighter localization. This is how SENCORP is intended to work. The last column of table 2 shows the number of members, K in the LE. For SENCORP this grows exponentially with Q, which was unaffordable for $N = 24$ and $Q = 4$, which is why we restricted $N = 16$.

The localized spatial correlation functions along the cross-hairs for temperature are shown in panels (c)-(e) of Fig. 7, which shows the localizing effect of SENCORP Exps. 4 and 5 (dotted and dashed lines respectively) against the unlocalized correlations (solid lines). All lines differ in the vicinity of the centre of the cross-hair (where correlations are close to unity) more so than for the spectral scheme in the corresponding panels of Fig. 3. As shown in

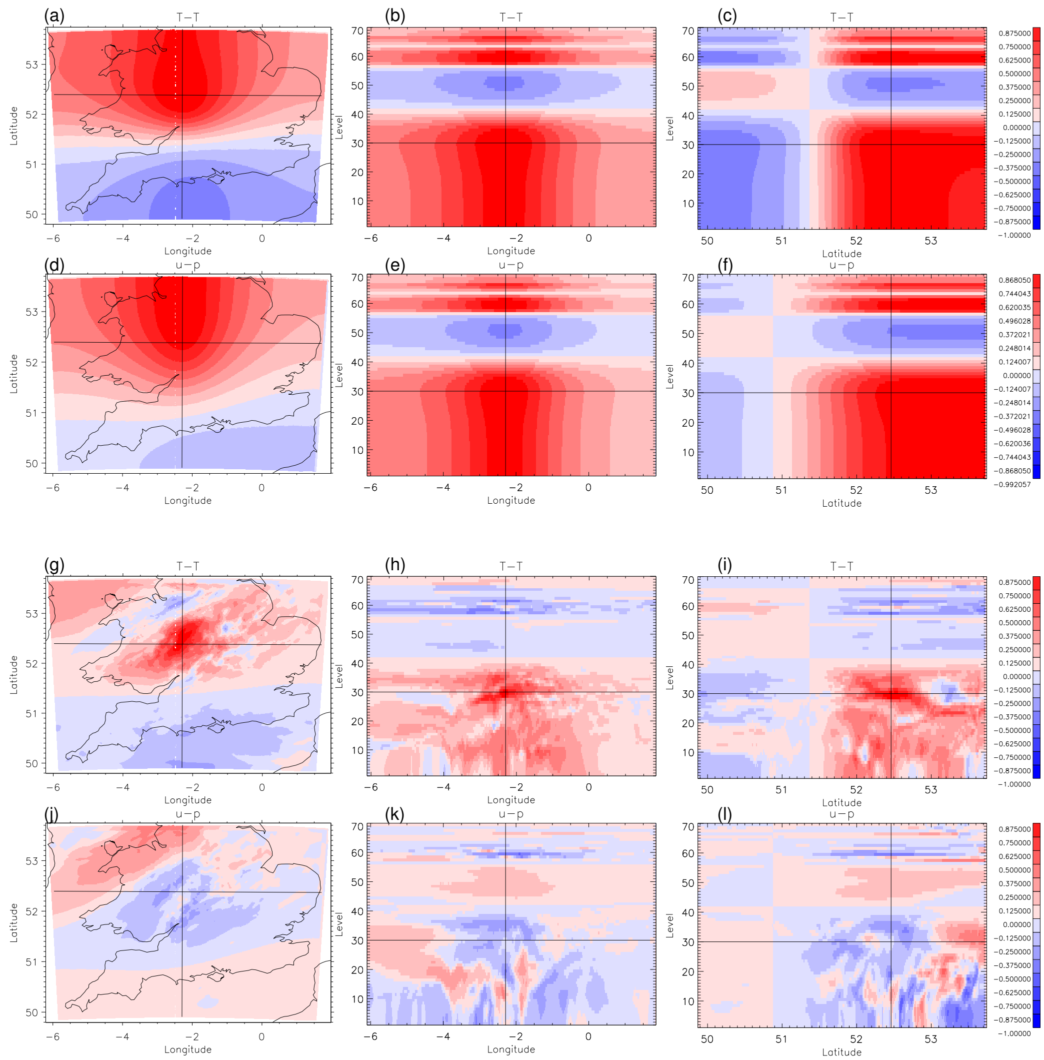

Figure 4: The upper panels, (a)-(f), are univariate and multivariate implied spatial moderation functions for the main case study for the spectral scheme (Exp. 1). The lower panels, (g)-(l) are the localized versions of Fig. 2 (i.e. Fig. 2 multiplied by the first set of six panels of this Fig.). The meaning of the cross-hair is explained in the caption of Fig. 2.

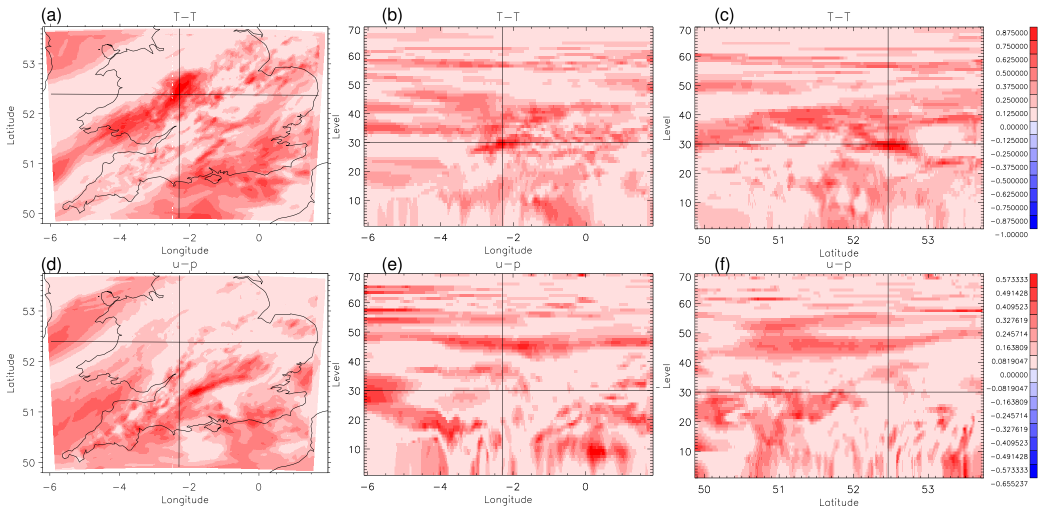

Figure 5: Univariate and multivariate implied spatial moderation functions for the main case study for the SENCORP scheme with $Q = 2$ (Exp. 4). The meaning of the cross-hair is explained in the caption of Fig. 2.

panels (a) and (b), the balance properties of the LE (for GB and HB) are virtually destroyed in these SENCORP experiments. There is evidence of correspondence between the target values (unlocalized) and the SENCORP values (in the sense that when the DE correlations increase so do the LE correlations), but the values are very different.

The effectiveness of SENCORP for $Q = 2$ and $Q = 4$ to localize is good, but their maintenance of balance properties is poor. Of these two experiments, $Q = 2$ gives (unsatisfactory but) better balance results. We perform an extra SENCORP experiment with $Q = 1$ (see footnote 7) to see how that configuration performs (Exp. 3). The results are included in Fig. 7 (dash-dotted lines). The GB and HB values (panels (a) and (b)) are closer to the target values than the previous SENCORP tests, but Exp. 3 remains unsatisfactory and, in any case, proves ineffective at localizing (panels (c)-(e)).

3.3.2 Effect of pre-smoothing

The full SENCORP scheme in [3] has more freedom to influence the length-scales than the simplified SENCORP (e.g. by making the parameter q mentioned in footnote 5 greater than unity). Here though we are able to pre-smooth the DE. Two further SENCORP experiments - Exps. 6 and 7 - are done with pre-smoothing of 10 and 50 grid points respectively in the horizontal and vertical directions. A summary of the results is in Fig. 8. These tests show that the pre-smoothing increases the localization length-scales (compared to no pre-smoothing), but no choice of pre-smoothing maintains balance properties close to the target values.

3.4 Diagnostics of the ECO-RAP scheme

The evaluation of the matrix of CE members for ECO-RAP (13) is more expensive in computer time than comparable spectral and SENCORP schemes. Equation (13) requires the computation of $\mathbf{C}^{\circ Q} \in \mathcal{R}^{n\times n}$ acting on a matrix that is $\in \mathcal{R}^{n\times K}$ which is a prohibitive task for typical n. In order to make ECO-RAP practical for the test cases used in this paper, some approximations

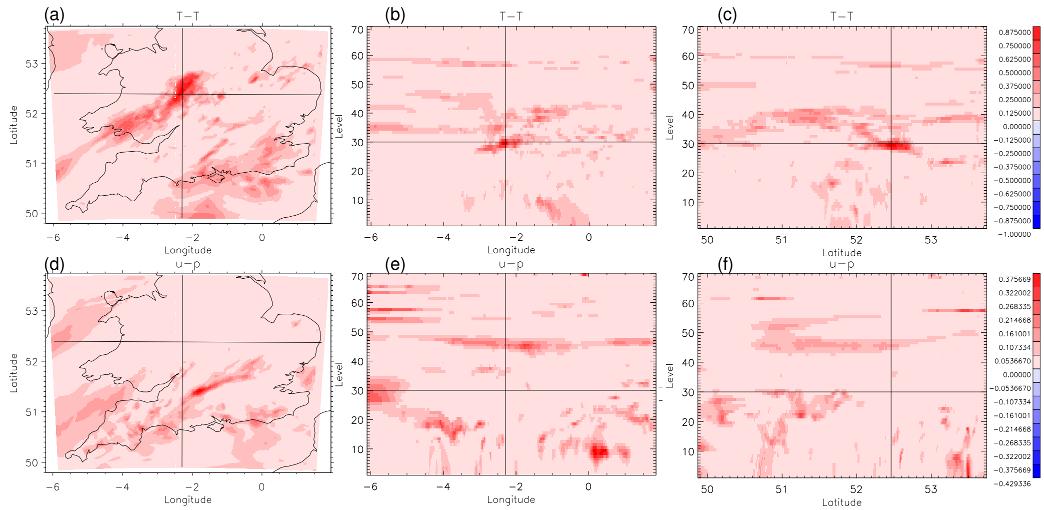

Figure 6: Univariate and multivariate implied spatial moderation functions for the main case study for the SENCORP scheme with $Q = 4$ (Exp. 5). The meaning of the cross-hair is explained in the caption of Fig. 2.

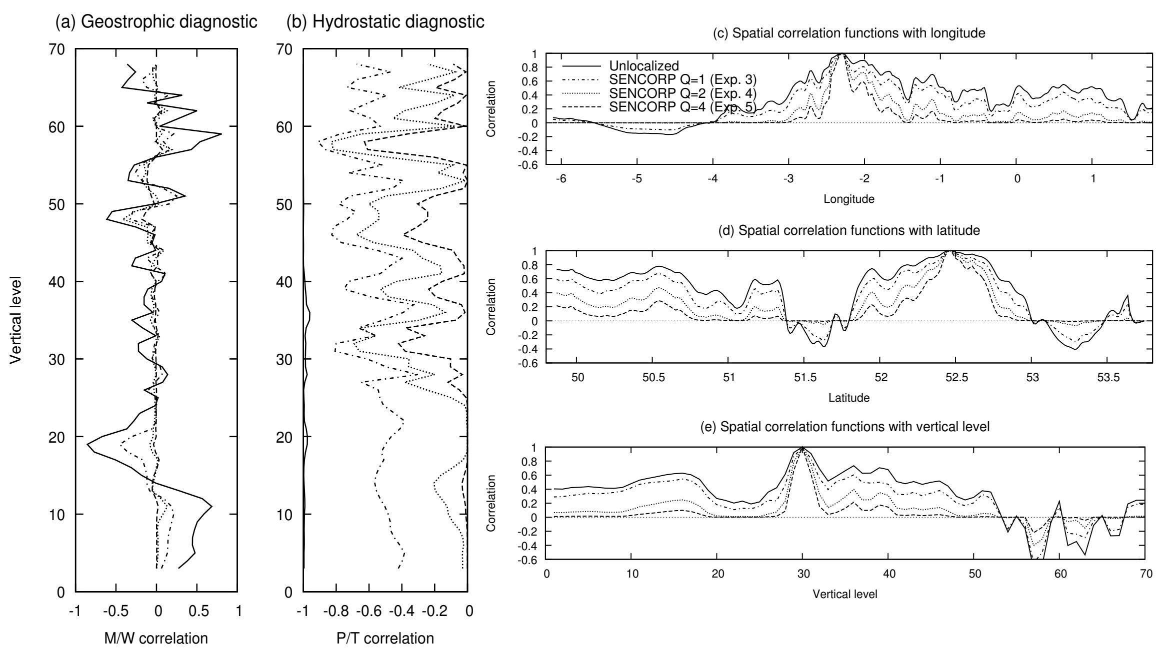

Figure 7: Diagnostics for the unlocalized and SENCORP scheme with $Q = 1$, 2 and 4 for the main case study (note $N = 16$). Panels (a) and (b): geostrophic and hydrostatic correlation diagnostics. Panels (c)-(e): spatial correlation functions with longitude, latitude and level. In all panels the continuous lines are for the unlocalized system ($N = 16$ version of Exp. 0), the dash-dotted lines are for $Q = 1$ (Exp. 3), the dotted lines are for $Q = 2$ (Exp. 4) and the dashed lines are for $Q = 4$ (Exp. 5).

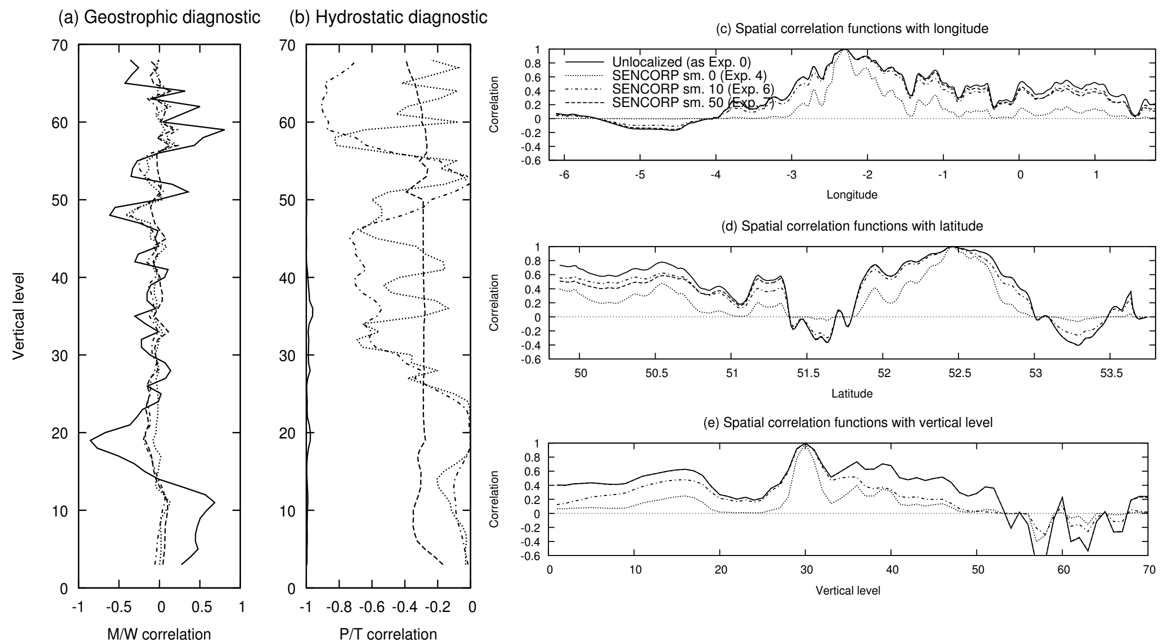

Figure 8: Diagnostics for the unlocalized and SENCORP scheme with different degrees of pre-smoothing to generate the SE for the main case study (note $N = 16$ and $Q = 2$). Panels (a) and (b): geostrophic and hydrostatic correlation diagnostics. Panels (c)-(e): spatial correlation functions with longitude, latitude and level. In all panels the continuous lines are for the unlocalized system ($N = 16$ version of Exp. 0), the dotted lines are for no pre-smoothing (Exp. 4, reproduced from Fig. 7), the dash-dotted lines are for 10 grid-points of pre-smoothing in the horizontal and vertical (Exp. 6) and the dashed lines are for 50 grid-points of pre-smoothing (Exp. 7).

to (13) are required. The full evaluation of $\mathbf{K}^{\mathrm{ECORAP}}$ (adapted from (14)) is:

$$[\mathbf{K}^{\mathrm{ECORAP}}]_{(\mathbf{r}s)\mathbf{k}} = [\boldsymbol{\omega}_{\mathbf{k}}]_{(\mathbf{r}s)} = c_{(\mathbf{r}s)} \sum_{s'} \sum_{r'_x=1}^{n_x} \sum_{r'_y=1}^{n_y} \sum_{r'_z=1}^{n_z} (\mathbf{C}^{\circ Q})_{(\mathbf{r}s)(\mathbf{r}'s')} \mathbf{F}_{(\mathbf{r}'s')\mathbf{k}} (\boldsymbol{\Lambda}_{s'}^{1/2})_{\mathbf{k}\mathbf{k}}, \tag{15}$$

where $\mathbf{r}' = (r'_x, r'_y, r'_z)$ and the domain has n_x, n_y and n_z points in the x, y and z directions respectively. Assuming that short-range correlations in $\mathbf{C}^{\circ Q}$ are the most important, (15) can be approximated by:

$$[\mathbf{K}^{\mathrm{ECORAP}}]_{(\mathbf{r}s)\mathbf{k}} = [\boldsymbol{\omega}_{\mathbf{k}}]_{(\mathbf{r}s)} \approx c_{(\mathbf{r}s)} \sum_{s'} \sum_{r'_x=r_x-\rho_{\mathrm{H}}}^{r_x+\rho_{\mathrm{H}}} \sum_{r'_y=r_y-\rho_{\mathrm{H}}}^{r_y+\rho_{\mathrm{H}}} \sum_{r'_z=r_z-\rho_{\mathrm{V}}}^{r_z+\rho_{\mathrm{V}}} (\mathbf{C}^{\circ Q})_{(\mathbf{r}s)(\mathbf{r}'s')} \mathbf{F}_{(\mathbf{r}'s')\mathbf{k}} (\boldsymbol{\Lambda}_{s'}^{1/2})_{\mathbf{k}\mathbf{k}}, \tag{16}$$

where ρ_{H} is the maximum distance in either of the horizontal directions of correlations considered in $\mathbf{C}^{\circ Q}$, and ρ_{V} is the maximum distance of the vertical correlations considered. In this paper we will call these the ECO-RAP influence parameters. Formulation (16) is used in this paper, so a number of experiments are performed with different values of ρ_{H} and ρ_{V} (columns 12 and 13 in table 2).

3.4.1 Effect of the ECO-RAP influence parameters

It was found by experimentation that the degree of GB exhibited by the LE produced by ECO-RAP degrades with increasing horizontal ECO-RAP influence parameter (not shown), so this was set to $\rho_{\mathrm{H}} = 0$ in the experiments shown here. We are left with a scheme that is essentially the spectral scheme in the horizontal and the ECO-RAP scheme in the vertical and is a significant saving of computer effort. This subsection is concerned with the effect of ρ_{V} only (all spectral parameters are as Exp. 1, the order is $Q = 2$ and only a small amount of pre-smoothing (two units) is done in the horizontal and vertical directions).

Figure 9 shows the localized balance and spatial correlation diagnostics for this configuration for five values of ρ_{V} (Exps. 8-12), compared with the unlocalized (Exp. 0) results. In terms of GB (panel (a)), ECO-RAP appears to perform reasonably. Although it is not as close to the target correlations as the spectral scheme (Fig. 3(a)), it shows similar patterns of behaviour in the vertical. The case with $\rho_{\mathrm{V}} = 2$ (light dotted line) performs better than cases for other values of ρ_{V}. The significant gain from ECO-RAP though is found in the HB diagnostics (panel (b)). Broadly speaking we find that the larger the value of ρ_{V} the closer the HB diagnostics are to the target values. The test with $\rho_{\mathrm{V}} = 2$ gives similar results to the spectral scheme (see Fig. 3(b)), but increasing this to $\rho_{\mathrm{V}} = 64$ (black dash-dotted line) improves the match to the target values throughout the middle levels of the domain (although marginally worst than the spectral scheme in the lowest levels). This is a result that might be expected since the larger ρ_{V}, the more flow-dependent the scheme is and the further away the scheme is from the pure spectral scheme. The horizontal localized correlation functions (panels (c) and (d)) show similar behaviour to the spectral case (see Fig. 3, panels (c) and (d)). This is not surprising as the horizontal aspects of the scheme are similar to the spectral scheme since $\rho_{\mathrm{H}} = 0$ (it is not identical because of mixing of information between vertical levels in ECO-RAP).

These results appear to be encouraging, but the localized vertical correlation functions (panel (c)) tell a different story. The vertical influence parameter value tested that gives the best results with regard to HB ($\rho_{\mathrm{V}} = 64$) leads to vertical correlations that are so similar to the unlocalized correlations that the scheme has become ineffective. The vertical influence parameter tested that gives the most effective localization is $\rho_{\mathrm{V}} = 2$, which, as we have shown above, does not preserve well the HB properties. By testing a range of ρ_{V} values shown in 9, we have though found that the value $\rho_{\mathrm{V}} = 24$ (black dashed line) is a possible compromise value, which approximately preserves GB and HB in most regions of the atmosphere (apart from vertical levels 40-55),

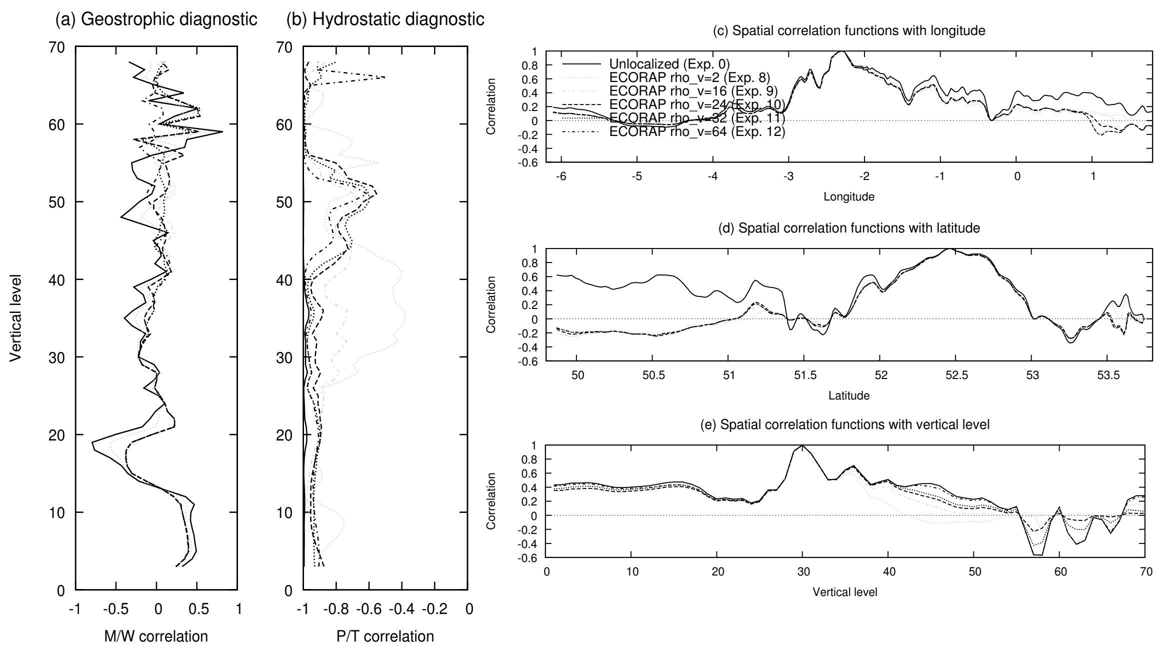

Figure 9: Diagnostics for the unlocalized and ECO-RAP scheme with different degrees of vertical influence parameter ρ_{V} for the main case study. Panels (a) and (b): geostrophic and hydrostatic correlation diagnostics. Panels (c)-(e): spatial correlation functions with longitude, latitude and level. In all panels the continuous lines are for the unlocalized system (Exp. 0), the light dotted lines are for $\rho_{\mathrm{V}} = 2$ (Exp. 8), the light dash-dotted lines are for $\rho_{\mathrm{V}} = 16$ (Exp. 9), the black dashed lines are for $\rho_{\mathrm{V}} = 24$ (Exp. 10), the black dotted lines are for $\rho_{\mathrm{V}} = 32$ (Exp. 11) and the black dash-dotted lines are for $\rho_{\mathrm{V}} = 64$ (Exp. 12).

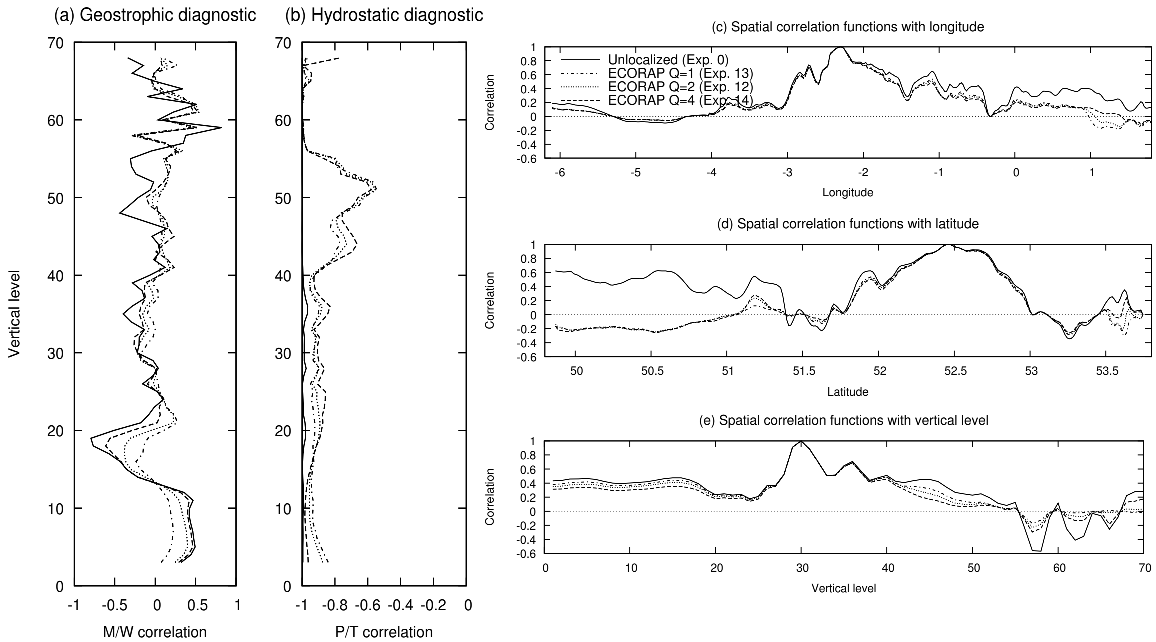

Figure 10: Diagnostics for the unlocalized and ECO-RAP scheme with $Q = 1$, 2 and 4 for the main case study (all runs have $\rho_{\mathrm{H}} = 0$ and $\rho_{\mathrm{V}} = 24$). Panels (a) and (b): geostrophic and hydrostatic correlation diagnostics. Panels (c)-(e): spatial correlation functions with longitude, latitude and level. In all panels the continuous lines are for the unlocalized system (Exp. 0), the dash-dotted lines are for $Q = 1$ (Exp. 13), the dotted lines are for $Q = 2$ (Exp. 12, reproduced from Fig. 9), and the dashed lines are for $Q = 4$ (Exp. 14).

while still being effective at reducing far-field correlations. Although the original reason for introducing the two influence parameters was for computational efficiency, their presence has shown how the ECO-RAP scheme can be tuned. We believe that these findings are potentially important for possible use in convective-scale ensemble DA.

3.4.2 Effect of the order, Q

Maintaining the best value, $\rho_{\mathrm{V}} = 24$, from Sect. 3.4.1, we now investigate the effect of changing the order of the scheme. Fig. 10 summarises the results for the same values of Q investigated for SENCORP in Sect. 3.3.1. There is no clear overall winner as all experiments show significant reduction of far-field correlations and have levels of HB that are closer to the target unlocalized values than other schemes. Most differences lie with the GB diagnostics where there is a general trend that the larger Q the better the match. For this reason we take Exp. 14 as the best result. By eye, the set of parameters represented by Exp. 14 seems to perform reasonably well with the diagnostics shown.

4 Other case studies

The results in Sect. 3 are for a single profile. To demonstrate further the performance of the schemes, we repeat the best configurations found from Sect. 3 to three additional profiles covering various meteorological conditions, including precipitating and non-precipitating conditions (see Tab. 3). Note that profile A is the one studied earlier. For conciseness, only the balance

Profile	Date	Time (UTC)	Long.	Lat.	Forecast lead time	Precip?	Details
A	20/09/2011	15:00	2.3°W	52.5°N	3 hr	Yes	On a cold front arriving from the west.
B	20/09/2011	15:00	0.3°W	51.0°N	3 hr	No	Ahead of the cold front.
C	26/07/2007	18:00	3.0°W	52.9°N	1 hr	Yes	Leeward of N.Wales orography.
D	26/07/2007	18:00	1.3°W	52.4°N	1 hr	No	Non-convecting region

Table 3: Characteristics of the four profiles used in this study.

diagnostics are shown here. According to our judgement, the best schemes for balance maintenance are represented by Exp. 1 (spectral), Exp. 3 (SENCORP) and Exp. 14 (ECO-RAP).

The GB comparison is shown in Fig. 11. The results are consistent with earlier results: all schemes maintain most of the GB characteristics of the profile except for SENCORP (dash-dotted lines). Even though ECO-RAP (dashed lines) doesn't quite capture all of the peaks and troughs in the GB diagnostic quite as well as the spectral scheme (dotted lines) - e.g. around levels 19 and 50 in panel (a), and levels 45 and 53 in panel (b) - this is possibly off-set by its performance in the HB diagnostic.

The HB comparison is shown in Fig. 12. The characteristics of the unlocalized system are clearly less closely followed across the board. SENCORP (dash-dotted lines) performs the least well, followed by the spectral scheme (dotted lines). Although ECO-RAP (dashed lines) matches the unlocalized HB characteristics the closest, overall it is not clear whether its performance is adequate in the upper levels, especially if it is used in a convective-scale setting. ECO-RAP often follows the ups and downs of the unlocalized diagnostic (but with lower degrees of HB), apart from at levels higher up in the atmosphere (e.g. around level 50 in panel (a), level 40 in panel (b) and levels 40 and 60 in panels (c) and (d)).

5 Discussion and conclusions

We have demonstrated how well the three Schur product-type localization schemes described in Sect. 2 are able to simultaneously remove (assumed) spurious correlations from finite-size ensembles and maintain the balance properties of the unlocalized ensemble. The three schemes have not been designed to specifically conserve balance, but have been considered before in the literature. They are based on (i) a decomposition of the moderation matrix in a spectral basis, (ii) a simplified version of SENCORP [3] and (iii) the ECO-RAP method [1]. Results are derived from a number of test ensembles of forecasts from the Met Office's MOGREPS system, adapted for convective-scale. This work shows how the balance properties of a localized covariance matrix can be extracted by constructing the 'localized ensemble' (Tab. 1) which has that covariance matrix and by studying the geostrophic balance (GB) and hydrostatic balance (HB) properties and comparing them to those of the 'dynamical ensemble' (the unlocalized ensemble).

Localization affects balances because multiplying by a moderation function that reduces with distance affects fields and gradients of fields in different ways [12] and balance is often defined as the equalization of a field (e.g. wind) and the derivative of another field (e.g. pressure). Longer localization length-scales ease this problem, but reduce the efficacy of the localization scheme. Although we could have reduced these problems by making a change of variable, and then localizing (e.g. [22]), we chose to localize directly in the model variables (u, v, p and T) as

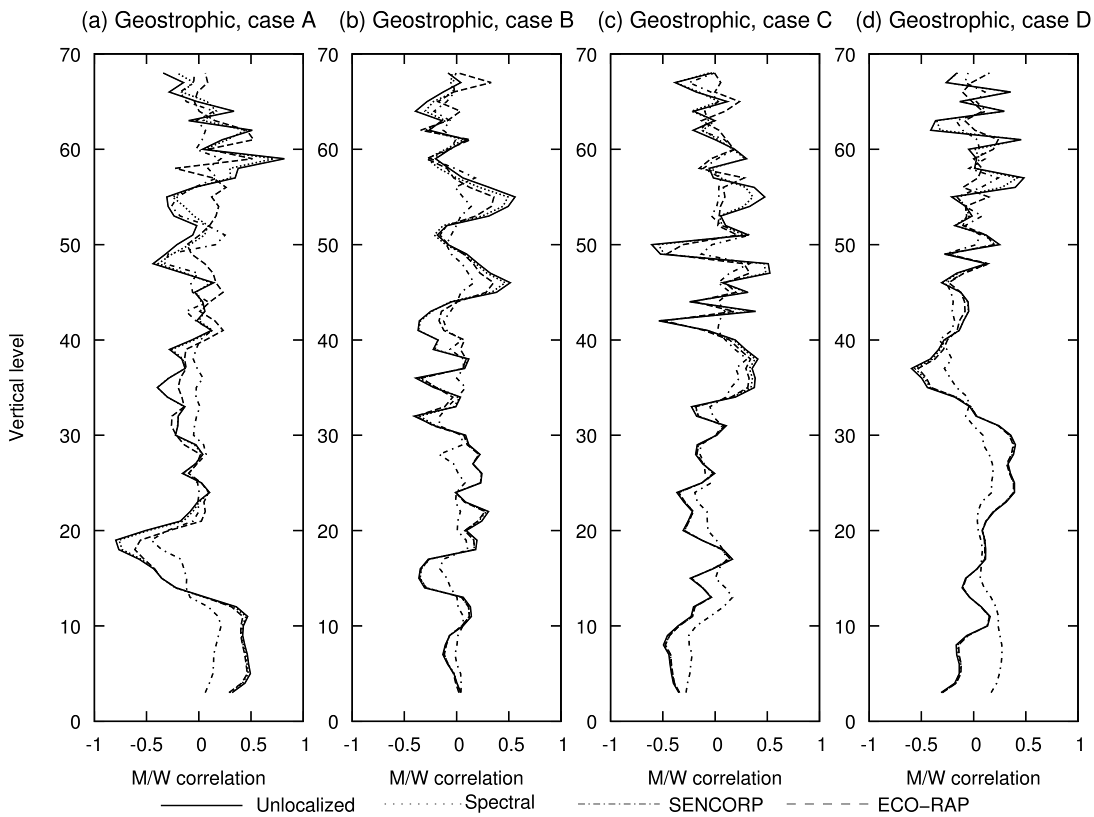

Figure 11: Geostrophic balance diagnostic for the four profile cases detailed in Tab. 3. In all panels, the continuous lines are for the unlocalized system (Exp. 0), the dotted lines are for the spectrally localized system (Exp. 1), the dash-dotted lines are for the SENCORP localized system (Exp. 3), and the dashed lines are for the ECO-RAP localized system (Exp. 14).

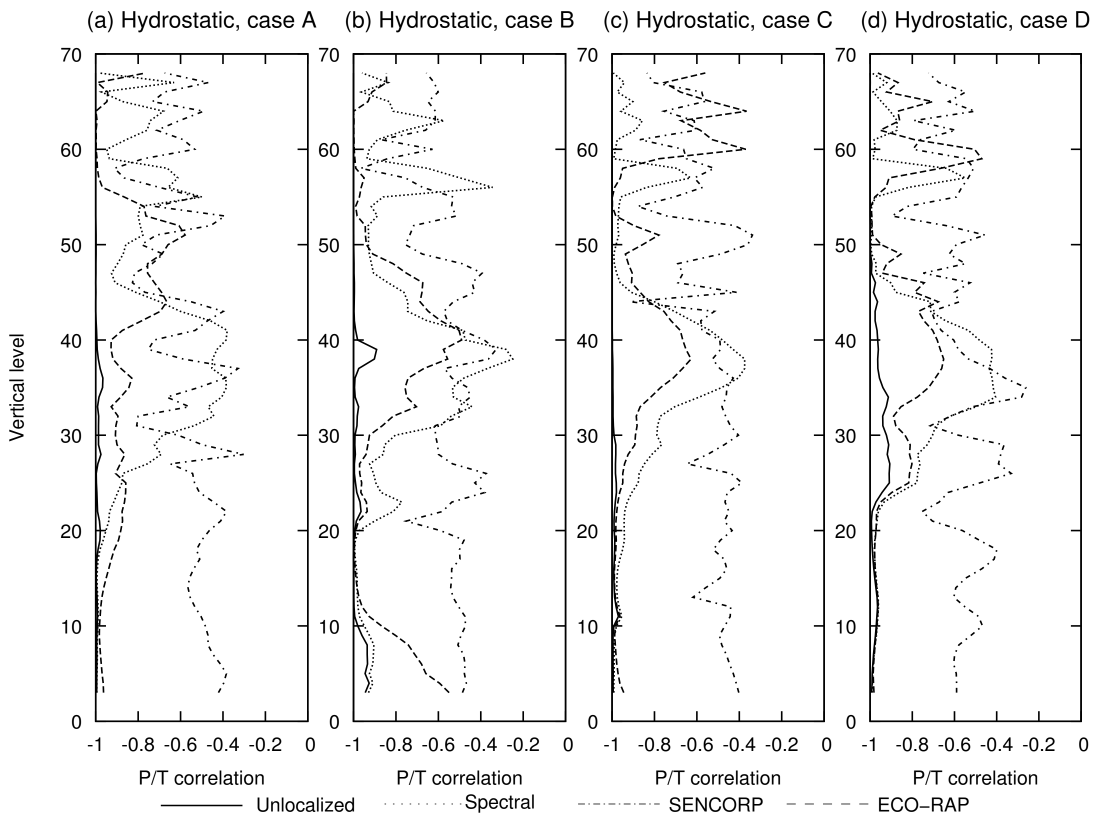

Figure 12: Hydrostatic balance diagnostic for the four profile cases detailed in Tab. 3. In all panels, the continuous lines are for the unlocalized system (Exp. 0), the dotted lines are for the spectrally localized system (Exp. 1), the dash-dotted lines are for the SENCORP localized system (Exp. 3), and the dashed lines are for the ECO-RAP localized system (Exp. 14).

we wanted to test the adaptive schemes rather than a change of variables. Adaptive localization schemes offer a possibility to overcome this problem as the degree of localization is dependent on the flow itself and not just on a prescribed moderation function. For instance a scheme might introduce moderation functions with longer length-scales locally where the ensemble correlations themselves show a longer length-scale, as we believe is the case for the two adaptive schemes here (SENCORP and ECO-RAP). Maintaining balance is found to be particularly difficult for HB, which is obeyed far more strongly than GB in the flows studied.

Out of the candidates there is no one scheme that maintains both GB and HB closely, but we do find that a particular configuration of ECO-RAP is the best scheme overall, which minimises inappropriate imbalance, but still is able to filter far-field correlations. Horizontal and vertical 'influence parameters' were invented for the $\mathbf{C}^{\circ Q}$ matrix. These were introduced for efficiency, but their use proved to be essential for ECO-RAP to give best results. SENCORP localizes very effectively, but it also destroys the balance properties the most.

We do acknowledge certain weaknesses of the tests performed in this paper. Weaknesses in the implementation of the schemes are as follows. The spectral and ECO-RAP schemes rely on a truncation in the horizontal and vertical wavenumber spectra which introduces artefacts in the implied moderation functions, such as non-reducing values in the vertical direction. We also find negative moderation function values although these affect mainly the far-field where the moderation functions are smaller anyway (we presume that the negative values are a consequence of truncation also). In parts of the schemes where length-scales have a prescribed element (spectral and ECO-RAP) we have used the same length-scales for all variables for simplicity. Even though, as stated above, the simplified SENCORP scheme is poor at maintaining balance, this result may say little about the performance of the full SENCORP scheme (see footnote 5). There are also potential weaknesses in the balance diagnostics, which are local measures of balance only and so susceptible to grid-scale noise (non-local balance diagnostics are considered, e.g., by [29], but they do not consider localization). Without implementing the schemes in a realistic ensemble data assimilation/forecasting system there is no quantitative indication of firstly how close the localized GB and HB diagnostics should be to the unlocalized diagnostics, and secondly how much localization is sufficient. It is hoped though that this work can help guide operational developers to the best localization scheme that can be trialled.

Acknowledgements

The authors of this work were funded by NERC (the Natural Environment Research Council) via the NCEO (National Centre for Earth Observation) and DIAMET (DIAbatic influences on Mesoscale structures in ExTratropical storms) programmes, and ESA (the European Space Agency). The authors would like to thank Jonathan Flowerdew (Met Office) for useful discussions and Simon Wilson (Met Office and National Centre for Atmospheric Science) for help in setting up the ensemble. We acknowledge use of the Met Office and MONSooN supercomputer systems (MONSooN is a collaborative facility supplied under the Joint Weather and Climate Research Programme, which is a strategic partner ship between the Met Office and NERC).

References

[1] Bishop C.H. and Hodyss D., Ensemble covariances adaptively localized with ECO-RAP, Part 1: Tests on simple error models, Tellus A 61, 84-96 (2009).

[2] Bishop C.H. and Hodyss D., Ensemble covariances adaptively localized with ECO-RAP, Part 2: A strategy for the atmosphere, Tellus A 61, 97-111 (2009).

[3] Bishop C.H. and Hodyss D., Flow adaptive moderation of spurious ensemble correlations and its used in ensemble-based data assimilation, Quart. J. Roy. Met. Soc. 133, 2029-2044 (2007), DOI:10.1002/qj.169.

[4] Zhu J., Zheng F. and Li X., A new localization implementation scheme for ensemble data assimilation of non-local observations, Tellus A (2010). DOI: 10.1111/j.1600-0870.2010.00486.x

[5] Ott E., Hunt B.R., Szunyough I., Zimin A.V., Kostelich E.J., Corazza M., Kalnay E., Patil D.J., Yorke J.A., A local ensemble Kalman Filter for atmospheric data assimilation, Tellus A 56, 415-428 (2004).

[6] Bannister R.N., A review of forecast error covariance statistics in atmospheric variational data assimilation. II: Modelling the forecast error covariance statistics, Q.J.R. Meteor. Soc. 134, 1971-1996 (2008).

[7] Bannister R.N., A review of forecast error covariance statistics in atmospheric variational data assimilation. I: Characteristics and measurements of forecast error covariances, Quart. J. Roy. Meteor. Soc. 134, 1951-1970 (2008).

[8] Evensen G., Sequential data assimilation with a non-linear quasi-geostrophic model using Monte Carlo methods to forecast error statistics, J. Geophys. Res. 99(C5): 10 143–10 162 (1994).

[9] Gaspari G. and Cohn S.E., Construction of correlation functions in two and three dimensions, Q.J.R. Meteor. Soc. 125 pp.723-757 (1999).

[10] Evensen G., The ensemble Kalman Filter: Theoretical formulation and practical implementation, Ocean Dynamics 53, 343-367 (2003).

[11] Houtekamer P.L. and Mitchell H.L., Data assimilation using an ensemble Kalman Filter technique, Mon. Wea. Rev. 129, 2776-2790 (1998).

[12] Lorenc A.C., The potential of the ensemble Kalman Filter for NWP - a comparison with 4D-VAR, Quart. J. Roy. Meteor. Soc. 129, 3183-3203 (2003).

[13] Bishop C.H., Etherton B.J. and Majumdar S.J., Adaptive sampling with the ensemble transform Kalman Filter. Part I: Theoretical aspects, Mon. Wea. Rev. 129, 420-436 (2001).

[14] Pham D.T., Verron J. and Rouband M.C., A singular evolutive extended Kalman filter for data assimilation in oceanography, J. Mar. Syst. 16, 323-340 (1998).

[15] Janjić T., Nerger L., Albertella A., Schröter, J. and Skachko S., On domain localization in ensemble-based Kalman filter algorithms, Mon. Wea. Rev. 139, 2046-2060 DOI:10.1175/2011MWR3552.1 (2011).

[16] Fertig E.J., Hunt B.R., Ott E., Szunyough I., Assimilating non-local observations with a local ensemble Kalman filter, Tellus 59A, 719-730 (2008).

[17] Bowler N.E., Arribas A., Mylne K.R., Robertson K.B. and Beare S.E, The MOGREPS short-range ensemble prediction system, Quart. J. Roy. Meteor. Soc. 134, 703-722 (2008).

[18] Baker L., Rudd A., Migliorini S. and Bannister R., Representation of model error in a convective-scale ensemble prediction system, Nonlinear Processes in Geophysics 21, 19-39, doi: 10.5194/npg-21-19-2014 (2014).

[19] Houtekamer P.L. and Mitchell H.L., Ensemble Kalman filtering, Quart. J. Roy. Meteor. Soc. 131, 3269-3289, DOI:10.1256/qj.05.135 (2005).

[20] Kirchgessner P. and Nerger L., On the choice of an optimal localization radius in ensemble Kalman filter methods, Mon. Wea. Rev. DOI:10.1175/MWR-D-13-00246.1 (2014).

[21] Pailleux J., Large-scale data assimilation systems: atmospheric applications to numerical weather prediction, J. Metero. Soc. Japan 75, 347-358 (1997).

[22] Kepert J.S., Covariance localization and balance in an ensemble Kalman filter, Quart. J. Roy. Meteor. Soc. 135, 1157-1176, DOI:10.1002/qj.443 (2009).

[23] Lorenc A.C., Ballard S.P., Bell R.S., Ingleby N.B., Andrews P.L.F., Barker D.M., Bray J.R., Clayton A.M., Dalby T., Li D., Payne T.J. and Saunders F.W., The Met Office global 3-dimensional variational data assimilation scheme. Q.J.R. Meteorol. Soc. 126, 2991-3012 (2000).

[24] Clayton A.M., Lorenc A.C. and Barker D.M., Operational implementation of a hybrid ensemble/4D-Var global data assimilation system at the Met Office, Q.J.R. Meteorol. Soc. 139, 1445-1461, DOI:10.1002/qj.2054 (2012).

[25] Migliorini S., Dixon M., Bannister R., Ballard S., Ensemble prediction for now-casting with a convection-permitting model - I: description of the system and the impact of radar-derived surface precipitation rates, Tellus 63, 464-496, DOI:10.1111/j.1600-0870.2010.00503.x (2011).

[26] Caron J.-F., Mismatching perturbations at the lateral boundaries in limited-area ensemble forecasting: A case study, Mon. Wea. Rev. 141, 356-374 (2013).

[27] Berre L., Estimation of synoptic and mesoscale forecast error covariances in a limited-area model, Mon. Wea. Rev. 128, 644-667 (2000).

[28] Bannister R.N., Migliorini S. and Dixon M. A. G., Ensemble prediction for now-casting with a convection-permitting model - II: forecast error statistics, Tellus 63A, 497-512 (2011).

[29] Vetra-Carvalho S., Dixon M., Migliorini S., Nichols N.K., Ballard S.P., Breakdown of hydrostatic balance at convective scales in the forecast errors in the Met Office Unified Model, Q.J.R. Meteor. Soc. 138, 1709-1720, DOI:10.1002/qj.1925 (2012).

[30] Golding B.W., Ballard S.P., Mylne K., Roberts N., Saulter A., Wilson C., Agnew P., Davis L.S., Trice J., Jones C., Simonin D., Li Z., Pierce C., Bennett A., Weeks M., and Moseley S., Forecasting Capabilities for the London 2012 Olympics, Bull. Amer. Meteor. Soc. 95, 883-896 (2014).